

Full length article

# First-principles study of the reconstruction of $MgM_2O_4$ ( $M = Mn, Fe, Co$ ) spinel surface

Tomoaki Kaneko<sup>a,\*</sup>, Yui Fujihara<sup>a,b,c,1</sup>, Hiroaki Kobayashi<sup>b,\*</sup>, Keitaro Sodeyama<sup>a,d,\*</sup><sup>a</sup> Research and Services Division of Materials Data and Integrated System (MaDIS), National Institute for Materials Science (NIMS), Namiki 1-1, Tsukuba, 305-0044, Japan<sup>b</sup> Institute of Multidisciplinary Research for Advanced Materials, Tohoku University, 2-1-1 Katahira, Sendai, 980-8577, Japan<sup>c</sup> Department of Chemistry, Graduate School of Science, 6-3 Aramaki-Aza-Aoba, Sendai, 980-8578, Japan<sup>d</sup> Element Strategy Initiative for Catalysts & Batteries (ESICB), Kyoto University, Nishikyo-ku, Kyoto, 615-8245, Japan

## ARTICLE INFO

## Keywords:

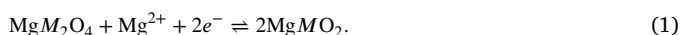
Mg-battery  
Cathode  
Spinel surface  
Surface reconstruction  
First-principles calculations

## ABSTRACT

$MgM_2O_4$  ( $M = Mn, Fe, Co$ ) spinels, which transform into rock-salt phases on Mg incorporation, are attractive cathode materials for future Mg battery applications. In this study, we investigated the energetics and reconstruction of  $MgM_2O_4$  ( $M = Mn, Fe, Co$ ) spinel surfaces using first-principles calculations. We found that the  $MgM_2O_4$  spinels stabilized when the Mg atoms in the topmost layer occupied the rock-salt-like sites. With an increase in the number of Mg atoms, the rock salt phase preferentially grew on the spinel surface rather than in the bulk. These features agree well with the core-shell growth of the rock-salt phase observed by recent aberration-corrected scanning transmission electron microscopy measurements.

## 1. Introduction

The development of high-energy-density rechargeable batteries is in great demand. Mg batteries, in particular, have attracted much interest owing to their high specific capacity (2200 mAh  $g^{-1}$ ) compared to conventional lithium-ion batteries (370 mAh  $g^{-1}$ ) [1,2]. Thus, the high rechargeability of Mg batteries makes them a potential option for our future energy storage needs. In Mg batteries,  $MgM_2O_4$  ( $M = Mn, Fe, Co$ )-based spinels (SPs) are considered promising cathode materials. During battery discharge, the SP transforms into the  $MgMO_2$  rock-salt (RS) phase, that is,



Although Mg batteries with an SP cathode exhibit high potential (2–3 V vs.  $Mg^{2+}/Mg$ ) and high capacities (260–270 mAh  $g^{-1}$ ), their poor reversibility and slow kinetics are critical problems impeding their application [1]. For the reversibility problem, the amount of Mg extracted is less than that of the Mg inserted, that is, the RS phase survives after charging. The purpose of this study was to investigate the stability of the RS phase at the  $MgM_2O_4$  SP surface using first-principles calculations.

Structural analysis of  $MgM_2O_4$  SPs has been performed by several authors [3,4]. Recently, Truong et al. performed an aberration-corrected scanning transmission electron microscopy (STEM) analysis of  $MgMn_2O_4$  (MMO) [3]. The observed STEM images showed a different atomic ordering at the MMO SP surface from that of the bulk region. They concluded that an RS phase layer was formed on the MMO SP surface. A similar structural transformation was observed for  $MgCo_2O_4$  (MCO) SP induced by electron irradiation without Mg incorporation [4]. In this case, the formation of a defective RS structure with cation site disorder was indicated. These findings help to identify ways of improving the performance of Mg batteries.

As an alternative to experiments, computational simulations based on density functional theory (DFT) is a powerful tool to investigate several properties of materials, such as atomic structure, electronic structure, energetics, and magnetic properties. However, computational studies concerning the surface of cathode materials in Mg batteries are limited. Jin et al. investigated the stabilities of MMO and  $MgNi_{0.5}Mn_{1.5}O_4$  SP surface [5]. Guo et al. systematically studied the stability of normal, mixed, and inverted  $MgFe_2O_4$  (MFO) SP surfaces [6,7]. Han et al. investigated the electronic properties of  $MgM_2O_4$  ( $M = Mn, Fe, Co$ ) surface to understand the reductive decomposition at the

\* Corresponding authors.

E-mail addresses: [KANeko.Tomoaki@nims.go.jp](mailto:KANeko.Tomoaki@nims.go.jp) (T. Kaneko), [hiroaki.kobayashi.c7@tohoku.ac.jp](mailto:hiroaki.kobayashi.c7@tohoku.ac.jp) (H. Kobayashi), [SODEYAMA.Keitaro@nims.go.jp](mailto:SODEYAMA.Keitaro@nims.go.jp) (K. Sodeyama).<sup>1</sup> Current affiliation: Energy Transformation Research Laboratory, Central Research Institute of Electric Power Industry, Nagasaka 2-6-1, Yokosuka, Kanagawa, 240-0196, Japan.

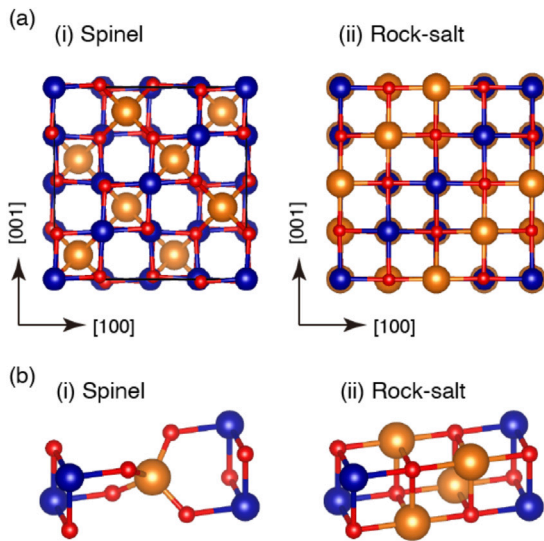


**Fig. 1.** (a) Lattice structure of (i) SP and (ii) RS. The orange, blue, and red balls represent Mg,  $M$  ( $M = \text{Mn, Fe, Co}$ ), and O atoms, respectively. In the side view, the  $8a$  sites of Mg can be seen at the interstitial sites, whereas the  $16c$  sites of Mg are overlapped by O and  $M$  atoms. (b) Local atomic configuration of (i) SP and (ii) RS.

cathode surface [8]. In their study, the lattice plane dependence was carefully investigated, whereas the possibility of reconstruction, which was observed experimentally [3,4], was not considered. Therefore, the RS phase growth in the SP phase is still unexplored. To understand the experimental results and accelerate future research, a computational study of the  $\text{MgM}_2\text{O}_4$  ( $M = \text{Mn, Fe, Co}$ ) SP surfaces can provide key insights. In this study, we investigated the energetics and reconstruction of  $\text{MgM}_2\text{O}_4$  SP surface by using first-principles calculations.

## 2. Methods

### 2.1. Computational details

In this study, we performed first-principles calculations based on DFT with a plane wave basis set within the spin polarized generalized gradient approximation (GGA) [9] using the quantum espresso code [10]. Ultrasoft pseudopotentials were used [11,12]. The semi-core states of 2s and 2p orbitals of Mg and 3s and 3p orbitals of Mn, Fe, and Co were also treated as valence electrons. For  $d$  orbitals of Mn, Fe, and Co, the isotropic type of DFT+ $U$  was adopted [13]. Mn, Fe, and Co have  $U_{\text{eff}}$  of 5.0, 5.0, and 6.0 eV, respectively, which are typical values for these elements, as summarized in the Supplemental Materials. The cutoff energy of the plane-wave basis set and the charge density were 35 and 315 Ry, respectively.

The lattice structures of the  $\text{MgM}_2\text{O}_4$  SP and  $\text{MgMO}_2$  RS are shown in Fig. 1(a). In the SP phase, the Mg atoms occupy  $8a$  sites of space group 227, that is, Mg is tetrahedrally coordinated. Conversely, in the RS phase, the Mg atoms occupy  $16c$  sites. We assumed antiferromagnetic ordering which is explained in detail in supplemental materials, whereas  $\text{Co}^{3+}$  ions in MCO do not have a magnetic moment. While MFO and MCO belong to the cubic lattice, MMO belongs to the tetragonal lattice because of the strong Jahn-Teller effect in MMO. The lattice constants of MMO were optimized using the stress tensor method within the cutoff energy of the plane wave basis set and charge density of 55 and 495 Ry, respectively, while cell parameters of MFO and MCO SP are determined by the total energy minimization. The threshold of stress is 0.1 kbar. To perform the calculations for a primitive cell, we used a special k-sampling of  $2 \times 2 \times 2$ .

As summarized in Table 1, the optimized lattice constants agree well with the experimental values, except for small deviations. We also

**Table 1**  
Results for bulk materials.

	$\text{MgMn}_2\text{O}_4$	$\text{MgFe}_2\text{O}_4$	$\text{MgCo}_2\text{O}_4$
$a_{\text{SP}}, c_{\text{SP}}$ (Å)	8.246, 9.637	8.602	8.203
Exp.	8.099, 9.284 <sup>a</sup>	8.397 <sup>b</sup>	8.138 <sup>c</sup>
Diff.	+1.8%, +3.8%	+2.4%	+0.8%
$a_{\text{RS}}$ (Å)	8.848	8.706	8.619
Exp.	8.672 <sup>d</sup>		8.503 <sup>c</sup>
Diff.	+ 2.0%		+1.4%
$V_{\text{Mg/Mg}^{2+}}$ (V)	2.20	1.86	2.75
Exp.	2.3 <sup>c</sup>	2.2 <sup>c</sup>	2.9 <sup>c</sup>

<sup>a</sup>Ref. [16].

<sup>b</sup>Ref. [17].

<sup>c</sup>Ref. [14].

<sup>d</sup>Ref. [3].

analyzed the RS phase of the  $\text{MgMO}_2$ . For simplicity, we assumed that the transition metal atoms remain at the same sites in the SP phase and that the Mg atoms occupy the  $16c$  sites in the RS phase. The voltage at the Mg metal anode is defined as:

$$V_{\text{Mg/Mg}^{2+}} = -\frac{1}{2e} [2E_{\text{MgMO}_2} - E_{\text{MgM}_2\text{O}_4} - E_{\text{Mg}}], \quad (2)$$

where  $E_{\text{MgMO}_2}$ ,  $E_{\text{MgM}_2\text{O}_4}$ , and  $E_{\text{Mg}}$  denote the total energies of RS, SP, and hcp-Mg per formula unit, respectively. The  $V_{\text{Mg/Mg}^{2+}}$  values obtained for Mn, Fe, and Co were 2.20, 1.86, and 2.75, respectively. These results agree well with the experimental results reported in Ref. Okamoto et al. [14], namely, 2.3 for Mn, 2.2 for Fe, and 2.9 for Co. The effect of  $U_{\text{eff}}$  on  $V_{\text{Mg/Mg}^{2+}}$  is summarized in the Supplementary Information. Note that the obtained  $V_{\text{Mg/Mg}^{2+}}$  depends on  $U_{\text{eff}}$ . Thus, a quantitative comparison between different SPs might be difficult. However, the electronic and structural properties of  $\text{MgM}_2\text{O}_4$  should be insensitive to variations in  $U$  by approximately 1 eV [15].

We considered the (001) cleaved slab models of SP, which consist of two periods of the primitive cell. As MMO exhibits lattice distortion caused by the Jahn-Teller effect, we considered the (001) and (100) surfaces of this material. For the calculations concerning the surfaces, we used a special k-sampling of  $2 \times 2 \times 1$ . An effective screening medium (ESM) was employed to remove spurious interactions between periodic images [18]. We introduced a vacuum layer of thickness greater than  $10 \text{ \AA}$  on both sides of the slab. For comparison, we also considered the RS phase formation in the bulk SP. In these calculations, we used a  $1 \times 1 \times 2$  supercell.

### 2.2. Surface termination

First, we discuss the surface models of  $\text{MgM}_2\text{O}_4$ . In the (001) direction, the atoms in the bulk SP were arranged as follows:

$$-M_4O_8 - \text{Mg}_2 - M_4O_8 - \text{Mg}_2 - M_4O_8 - \text{Mg}_2 - . \quad (3)$$

In this study, we considered two slab models, as shown in Fig. 2(a), one with an asymmetric cut and the other with a symmetric cut. In the asymmetrically cut model, the slab was cleaved between the  $4M_8O$  and  $2Mg$  layers, that is,

$$M_4O_8 - \text{Mg}_2 - M_4O_8 - \text{Mg}_2 - M_4O_8 - \text{Mg}_2. \quad (4)$$

By contrast, in the symmetrically cut model, the slab was cleaved across the Mg layers, and the Mg atoms were equally arranged at the top and bottom sides of the slab model, that is,

$$\text{Mg} - M_4O_8 - \text{Mg}_2 - M_4O_8 - \text{Mg}_2 - M_4O_8 - \text{Mg}. \quad (5)$$

In the following, we investigated the stability of these slab models by considering the effect of surface reconstruction.

Fig. 2(b) shows the reconstructions of the SP surfaces. At the SP surface, there are four  $16c$  sites on each side of the surface unit cell,

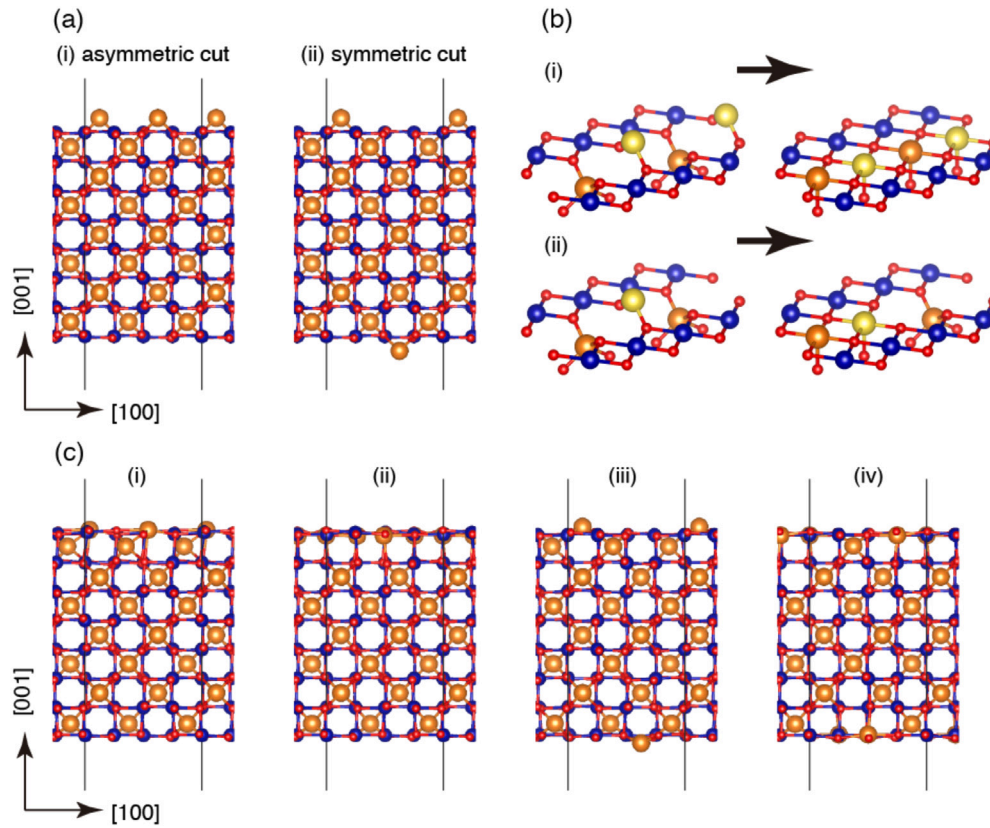
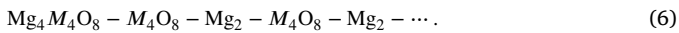
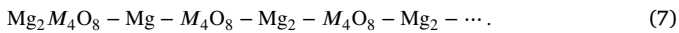


Fig. 2. Surface model of MCO: (a) Effect of cutting position. (b) Schematics of surface reconstructions. The surface Mg atoms are highlighted in yellow. (c) Optimized structures for MCO. Panels (i) and (ii) show the slab model with an asymmetric cut, and panels (iii) and (iv) show the slab model with a symmetric cut. The upper side of (ii) and both sides of (iv) are reconstruction models.

which are referred to as RS-like sites. In the asymmetrically cut model, as schematically shown in Fig. 2(b)–(i), two surface Mg atoms and two subsurface Mg atoms occupy four surface RS-like sites, that is,



Conversely, in the symmetrically cut model, one surface Mg atom occupies the surface RS-like site, which pulls a subsurface Mg atom to another surface RS-like site, as shown in Fig. 2(b)–(ii), that is,



It should be noted that the Mg atoms located at the RS-like sites are five-fold coordinated, whereas the surface and subsurface Mg atoms in the SP surface are two- and four-fold coordinated, respectively.

### 3. Results and discussion

#### 3.1. Surface reconstruction

The optimized structure of MCO is shown in Fig. 2(c). The optimized structures of the other two  $\text{MgM}_2\text{O}_4$  SPs are summarized in the Supplemental Materials. We considered the pristine surface and the RS-reconstructed surface for both the asymmetrically and symmetrically cut slabs. For the pristine surface structures, the Mg atoms closest to the surface shrink and tend to reach the RS-like sites.

Next, we discussed the energetics of the surface models. The surface energy is defined as follows:

$$\gamma = \frac{E_{\text{surf}} - E_{\text{bulk}}}{2S}, \quad (8)$$

where  $S$  denotes the area of the surface model,  $E_{\text{surf}}$  denotes the total energy of the surface, and  $E_{\text{bulk}}$  denotes the total energy of the bulk with the number of atoms being the same as the surface model. The obtained surface energies are summarized in Table 2. Although the surface energy is defined for the symmetric slab mode, that for the asymmetric slab model can be understood as the average of surface energy over the top and bottom surfaces of the slab [19].

We found that the surface with the RS-like reconstruction was more stable than the pristine surface, except for  $\text{MMO}(100)$  with an asymmetric cut. In the  $\text{MMO}(100)$  model, the surface unit cell was deformed from the square shape owing to the Jahn–Teller effect, which might destabilize the Mg atoms at the RS-like sites on the surface. The RS reconstruction with a symmetric cut was found to be the most stable, irrespective of the transition metal element type. For these stabilization, the increase of coordination number of Mg ions presumably plays an important role.

An RS-like reconstruction can be realized without the addition of extra Mg atoms. Therefore, the experimentally observed RS phase at the surface of SP should be off-stoichiometric, that is, the number of Mg atoms should be higher than that of  $\text{MgM}_2\text{O}_4$ . Next, we examined the growth of the RS phase by increasing the number of Mg atoms.

#### 3.2. Mg incorporation and RS phase growth

For this purpose, we defined the Mg incorporation energy as follows:

$$E_{\text{inc}} = \frac{E_{\text{SP}+n\text{Mg}} - E_{\text{SP}} - nE_{\text{Mg}}}{n}, \quad (9)$$

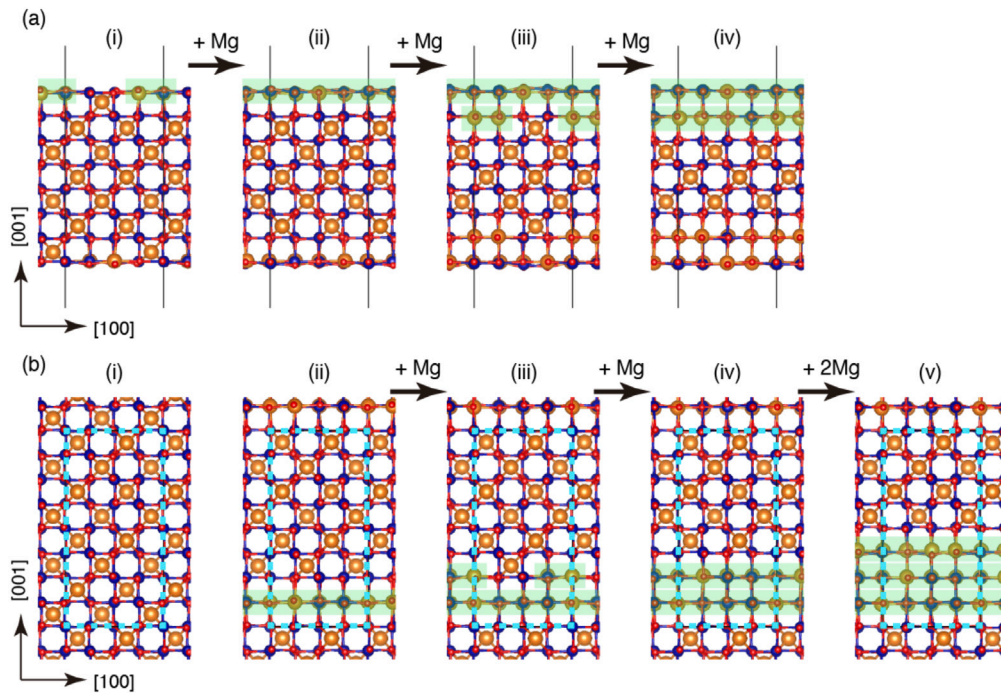


**Fig. 3.** Model of Mg incorporation: (a) Mg incorporation on the MCO surface. The light-green shades represent the RS-like phase. (b) Mg incorporation into the bulk MCO. The unit cells are indicated by cyan dotted lines.

**Table 2**  
Calculated results of surface energies,  $\gamma$  (eV/Å<sup>2</sup>).

	MMO(001)	MMO(100)	MFO(001)	MCO(001)
Asymmetric, pristine	0.0538	0.0669	0.0750	0.1035
Asymmetric, RS reconstructed	0.0485	0.0699	0.0700	0.0973
Symmetric, pristine	0.0521	0.0689	0.0703	0.1097
Symmetric, RS reconstructed	0.0338	0.0628	0.0578	0.0823

**Table 3**  
Calculated results of Mg incorporation energies,  $E_{inc}$  (eV/Mg).

	MMO(001)	MMO(100)	MFO(001)	MCO(001)
Surface	+1Mg -3.733	-3.826	-3.246	-4.263
Mg incorporation	+2Mg -3.753	-4.418	-3.820	-4.653
(eV/Mg)	+3Mg -3.789	-4.191	-3.655	-4.032
Bulk	+1Mg -1.728	-1.733	-1.319	-0.953
Mg incorporation	+2Mg -2.689	-2.672	-2.314	-2.342
(eV/Mg)	+4Mg -3.259	-3.241	-2.995	-2.631
Fully magnesiated RS	-4.402	-4.402	-3.724	-5.510

where  $n$  denotes the number of additional Mg atoms,  $E_{SP+nMg}$  denotes the total energy with  $n$  extra Mg atoms,  $E_{SP}$  denotes the total energy of SP. For a fully magnesiated SP, that is, for the RS phase,  $E_{inc}$  is given by  $-2 \text{ eV}_{Mg/Mg^{2+}}$ .

In this study, we used the symmetrically cut slab model for simplicity. We added Mg atoms near both sides of the surface RS-like sites. The structures obtained for MCO are shown in Fig. 3(a), where the grown RS phases are highlighted in light green.

The calculated Mg incorporation energies are summarized in Table 3. The obtained  $E_{inc}$  values are negative, indicating that the Mg insertion was exothermic. However, the absolute values of the reaction energies of Mg insertion are slightly smaller than or comparable to those for the bulk case, that is, the fully magnesiated RS case.

Next, we considered the RS phase growth in the bulk SP. The Mg incorporation model is schematically illustrated in Fig. 3(b). With the movement of four adjacent Mg atoms from 8a sites to 16c sites, a single-layer RS phase can be generated in the bulk SP without introducing

Mg atoms, as shown in Fig. 3(b)-(ii). This process was endothermic by 3.813, 2.311, 2.822, and 2.343 eV/unit cell for MMO(001), MMO(100), MFO(001), and MCO(001), respectively. As we explained in Section 2.2, the distance between nearest 16c and 8a sites is too short to occupy the two Mg ions. Then, strong repulsive forces make the Mg ion at 16c to empty 8a site. Therefore, the formation of a single-layer RS phase is necessary to model the RS phase growth in the bulk SP.

The calculated  $E_{inc}$  values for the bulk case are summarized in Table 3. With the introduction of one Mg atom, the  $E_{inc}$  values obtained were  $-1.7$ ,  $-1.3$ , and  $-1.0$  for MMO, MFO, and MCO, respectively, indicating that magnesianation preferentially occurs at the surface of SP. The effect of lattice distortion on the magnesianation energy was estimated for MCO SP with four Mg incorporation by changing the perpendicular cell parameter. As the result was shown in Supplemental Materials, the cell parameter change is 0.1 Angstrom, and the change in magnesianation energy should be of order of 0.1 eV at most. Although  $E_{inc}$  decreases monotonically with an increase in the number of Mg atoms, the absolute value of the reaction energy is much smaller than that for the surface. As the initial growth of the RS phase is energetically unfavorable, the RS phase cannot overcome the surface reaction energy. In other words, the RS-like reconstruction effectively lowered the energy barrier of the RS phase nucleation. Therefore, we can conclude that the RS phase grew on the surface of SP.

Recent STEM measurements showed the formation of RS phase on SP [3,4]. Our results agreed well with the experimental results reported by Truong et al. for the MMO surface [3]. The MCO SP transformed into defective RS with cation disorder, as observed by Okamoto et al. and electron beam irradiation was realized without Mg incorporation [4]. However, it seems difficult to draw firm conclusions from the calculations. More recently, RS phase formation on the SP surface was reported for MgCrMnO<sub>4</sub> SP [20,21]. Although we did not perform calculations for MgCrMnO<sub>4</sub> SP surface, we can speculate that a similar trend in energetic stability will be valid for MgCrMnO<sub>4</sub> SP.

As we mentioned in the introduction, the reversibility of Mg-battery with SP cathode is not acceptable for practical application. Our results and experimentally observed RS-phase on SP surfaces imply that Mg ions are fixed at the surface region due to high stability. Then, we can

presume that RS-phase formation on SP surfaces might prohibit Mg diffusion and demagnetization from SP. However, the simulations on diffusion of Mg ions in SP and RS would be necessary to conclude it, which is beyond the scope of the present paper.

In our calculations, we calculated the final structures of each magnetization reaction. Each reaction path contains Mg ion adsorption and migration processes, which have not negligible energy barriers. However, the calculations of energy barriers beyond the scope of the paper, since these processes are not uniquely determined.

#### 4. Summary

In this study, we investigated the energetics and reconstruction of  $MgM_2O_4$  ( $M = Mn, Fe, Co$ ) spinel surfaces using first-principles calculations. We found that the rock-salt-like reconstruction of the spinel surfaces in the (001) direction stabilized the system, irrespective of the transition metal element. We also found that the growth of the rock-salt phase preferentially occurred at the surface of the spinel compared to the bulk. As the formation of a single-layer rock-salt phase was endothermic, the growth of the rock salt phase in the bulk spinel was energetically unfavorable. The rock-salt-like reconstruction effectively lowered the energy barrier of the rock-salt phase nucleation. These results are in good agreement with a recent experiment performed using aberration-corrected scanning transmission electron microscopy.

#### CRediT authorship contribution statement

**Tomoaki Kaneko:** Investigation, Methodology, Writing – original draft. **Yui Fujihara:** Resources, Investigation. **Hiroaki Kobayashi:** Project administration, Funding acquisition. **Keitaro Sodeyama:** Conceptualization, Supervision, Funding acquisition.

#### Declaration of competing interest

The authors declare that they have no known competing financial interests or personal relationships that could have appeared to influence the work reported in this paper.

#### Data availability

Data will be made available on request.

#### Acknowledgments

The authors would like to thank Yoshitaka Tateyama and Masanobu Nakayama for the fruitful discussions. The calculations were carried out on the Numerical Materials Simulator at NIMS and the ITO supercomputer at Research Institute for Information Technology, Kyushu University. This research was partially supported by JST, Japan ALCA-SPRING Grant Nos. JPMJAL1301, Japan.

#### Appendix A. Supplementary data

Supplementary material related to this article can be found online at <https://doi.org/10.1016/j.apsusc.2022.156065>.

#### References

- [1] K. Shimokawa, T. Ichitsubo, Spinel–rocksalt transition as a key cathode reaction toward high-energy-density magnesium rechargeable batteries, *Curr. Opin. Electrochem.* 21 (2020) 93–99, <http://dx.doi.org/10.1016/j.coelec.2020.01.017>, <https://www.sciencedirect.com/science/article/pii/S2451910320300247>.
- [2] H. Kobayashi, K. Samukawa, M. Nakayama, T. Mandai, I. Honma, Promoting reversible cathode reactions in magnesium rechargeable batteries using metastable cubic  $mgmn_2o_4$  spinel nanoparticles, *ACS Appl. Nano Mater.* 4 (2021) 8328–8333, <http://dx.doi.org/10.1021/acsanm.1c01519>, arXiv:<https://doi.org/10.1021/acsanm.1c01519>.
- [3] Q.D. Truong, M.Kempaiiah, Devaraju, P.D. Tran, Y. Gambe, K. Nayuki, Y. Sasaki, I. Honma, Unravelling the surface structure of  $mgmn_2o_4$  cathode materials for rechargeable magnesium-ion battery, *Chem. Mater.* 29 (2017) 6245–6251, <http://dx.doi.org/10.1021/acs.chemmater.7b01252>, arXiv:<https://doi.org/10.1021/acs.chemmater.7b01252>.
- [4] N.L. Okamoto, K. Shimokawa, H. Tanimura, T. Ichitsubo, Feasible transformation of  $mgco_2o_4$  from spinel to defect rocksalt structure under electron irradiation, *Scr. Mater.* 167 (2019) 26–30, <http://dx.doi.org/10.1016/j.scriptamat.2019.03.034>, <http://www.sciencedirect.com/science/article/pii/S1359646219301770>.
- [5] W. Jin, G. Yin, Z. Wang, Y. Fu, Surface stability of spinel  $mgni_0.5mn_1.5o_4$  and  $mgmn_2o_4$  as cathode materials for magnesium ion batteries, *Appl. Surf. Sci.* 385 (2016) 72–79, <http://dx.doi.org/10.1016/j.apsusc.2016.05.096>, <http://www.sciencedirect.com/science/article/pii/S0169433216311151>.
- [6] H. Guo, A.C. Marschilok, K.J. Takeuchi, E.S. Takeuchi, P. Liu, Rationalization of diversity in spinel  $mgfe_2o_4$  surfaces, *Adv. Mater. Interfaces* 6 1901218 <http://dx.doi.org/10.1002/admi.201901218>, <https://onlinelibrary.wiley.com/doi/abs/10.1002/admi.201901218>.
- [7] H. Guo, J.L. Durham, A.B. Brady, A.C. Marschilok, E.S. Takeuchi, K.J. Takeuchi, P. Liu, Essential role of spinel  $MgFe_2O_4$  surfaces during discharge, *J. Electrochem. Soc.* 167 (2020) 090506, <http://dx.doi.org/10.1149/1945-7111/ab7f89>.
- [8] J. Han, S. Yagi, H. Takeuchi, M. Nakayama, T. Ichitsubo, Catalytic mechanism of spinel oxides for oxidative electrolyte decomposition in mg rechargeable batteries, *J. Mater. Chem. A* 9 (2021) 26401–26409, <http://dx.doi.org/10.1039/D1TA08115B>.
- [9] J.P. Perdew, K. Burke, M. Ernzerhof, Generalized gradient approximation made simple [phys. rev. lett. 77, 3865 (1996)], *Phys. Rev. Lett.* 78 (1997) 1396, <http://dx.doi.org/10.1103/PhysRevLett.78.1396>, <https://link.aps.org/doi/10.1103/PhysRevLett.78.1396>.
- [10] P. Giannozzi, O. Andreussi, T. Brumme, O. Bunau, M.B. Nardelli, M. Calandra, R. Car, C. Cavazzoni, D. Ceresoli, M. Cococcioni, N. Colonna, I. Carnimeo, A.D. Corso, S. de Gironcoli, P. Delugas, R.A.D. Jr., A. Ferretti, A. Floris, G. Fratesi, G. Fugallo, R. Gebauer, U. Gerstmann, F. Giustino, T. Gorni, J. Jia, M. Kawamura, H.Y. Ko, A. Kokalj, M. Küçükbenli, M. Marsili, N. Marzari, F. Mauri, N.L. Nguyen, H.V. Nguyen, A.O. de-la Roza, L. Paulatto, S. Poncè, D. Rocca, R. Sabatini, B. Santra, M. Schlipf, A.P. Seitsonen, A. Smogunov, I. Timrov, T. Thonhauser, P. Umari, N. Vast, X. Wu, S. Baroni, Advanced capabilities for materials modelling with quantum espresso, *J. Phys.: Condens. Matter* 29 (2017) 465901.
- [11] D. Vanderbilt, Soft self-consistent pseudopotentials in a generalized eigenvalue formalism, *Phys. Rev. B* 41 (1990) 7892–7895, <http://dx.doi.org/10.1103/PhysRevB.41.7892>, <https://link.aps.org/doi/10.1103/PhysRevB.41.7892>.
- [12] K.F. Garrity, J.W. Bennett, K.M. Rabe, D. Vanderbilt, Pseudopotentials for high-throughput dft calculations, *Comput. Mater. Sci.* 81 (2014) 446–452, <http://dx.doi.org/10.1016/j.commatsci.2013.08.053>, <http://www.sciencedirect.com/science/article/pii/S0927025613005077>.
- [13] M. Cococcioni, S. de Gironcoli, Linear response approach to the calculation of the effective interaction parameters in the LDA+U method, *Phys. Rev. B* 71 (2005) 035105, <http://dx.doi.org/10.1103/PhysRevB.71.035105>, <https://link.aps.org/doi/10.1103/PhysRevB.71.035105>.
- [14] S. Okamoto, T. Ichitsubo, T. Kawaguchi, Y. Kumagai, F. Oba, S. Yagi, K. Shimokawa, N. Goto, T. Doi, E. Matsubara, Intercalation and push-out process with spinel-to-rocksalt transition on mg insertion into spinel oxides in magnesium batteries, *Adv. Sci.* 2 1500072 <http://dx.doi.org/10.1002/advs.201500072>.
- [15] A. Schrön, C. Rödl, F. Bechstedt, Crystalline and magnetic anisotropy of the 3d-transition metal monoxides mno, feo, coo, and nio, *Phys. Rev. B* 86 (2012) 115134, <http://dx.doi.org/10.1103/PhysRevB.86.115134>, <https://link.aps.org/doi/10.1103/PhysRevB.86.115134>.
- [16] Z. Feng, X. Chen, T.T. Fister, M.J. Bedzyk, P. Fenter, Phase control of mn-based spinel films via pulsed laser deposition, *J. Appl. Phys.* 120 (2016) 015307, <http://dx.doi.org/10.1063/1.4955135>, arXiv:<https://doi.org/10.1063/1.4955135>.
- [17] S.M. Antao, I. Hassan, J.B. Parise, Cation ordering in magnesioferrite,  $mgfe_2o_4$ , to 982 ° C using in situ synchrotron x-ray powder diffraction, *Am. Mineral.* 90 (2005) 219–228, <http://dx.doi.org/10.2138/am.2005.1559>.
- [18] M. Otani, O. Sugino, First-principles calculations of charged surfaces and interfaces: A plane-wave nonrepeated slab approach, *Phys. Rev. B* 73 (2006) 115407, <http://dx.doi.org/10.1103/PhysRevB.73.115407>, <https://link.aps.org/doi/10.1103/PhysRevB.73.115407>.

- [19] S. Kim, M. Aykol, C. Wolverton, Surface phase diagram and stability of (001) and (111)  $\text{LiMn}_2\text{O}_4$  spinel oxides, *Phys. Rev. B* 92 (2015) 115411, <http://dx.doi.org/10.1103/PhysRevB.92.115411>, <https://link.aps.org/doi/10.1103/PhysRevB.92.115411>.
- [20] B.J. Kwon, L. Yin, H. Park, P. Parajuli, K. Kumar, S. Kim, M. Yang, M. Murphy, P. Zapol, C. Liao, T.T. Fister, R.F. Klie, J. Cabana, J.T. Vaughey, S.H. Lapidus, B. Key, High voltage mg-ion battery cathode via a solid solution cr–mn spinel oxide, *Chem. Mater.* 32 (2020) 6577–6587, <http://dx.doi.org/10.1021/acs.chemmater.0c01988>, arXiv:<https://doi.org/10.1021/acs.chemmater.0c01988>.
- [21] P. Parajuli, H. Park, B.J. Kwon, J. Guo, B. Key, J.T. Vaughey, P. Zapol, R.F. Klie, Direct observation of electron beam-induced phase transition in  $\text{mgcrmn}_4$ , *Chem. Mater.* 32 (2020) 10456–10462, <http://dx.doi.org/10.1021/acs.chemmater.0c03121>, arXiv:<https://doi.org/10.1021/acs.chemmater.0c03121>.